Experimental assessment of low velocity impact damage in flax fabrics reinforced biocomposites by coupled high-speed imaging and DIC analysis

Karthik Ram Ramakrishnan, Stéphane Corn, Nicolas Le Moigne, Patrick Ienny, Pierre Slangen

Experimental assessment of low velocity impact damage in flax fabrics reinforced biocomposites by coupled high-speed imaging and DIC analysis

Karthik Ram Ramakrishnan [a,b,*], Stéphane Corn [a,*], Nicolas Le Moigne [c], Patrick Ienny [a], Pierre Slangen [d]

[a] LMGC, IMT Mines Ales, Univ Montpellier, CNRS, Alès, France
[b] Faculty of Engineering and Natural Sciences, Tampere University, Tampere 33014, Finland
[c] Polymers Composites and Hybrids (PCH), IMT Mines Ales, Alès, France[1]
[d] EuroMov Digital Health in Motion, Univ Montpellier, IMT Mines Ales, Alès, France

A B S T R A C T

Structural composite materials with good impact resistance are required in several industrial sectors to design parts submitted to crashes or falling objects. This work investigates the impact behaviour of flax fabrics-epoxy and commingled flax-polypropylene (PP) fibres composite plates manufactured using compression moulding process. An instrumented drop tower was used to conduct low velocity impact tests at several energies and high-speed imaging coupled with DIC analysis was used to assess the damage evolution. A crack-tracking algorithm was implemented in ImageJ to identify the initiation and propagation of cracks. A comparison of the force-displacement histories and high-speed camera results for both composites were used to identify the different modes of damage and the critical energy for complete penetration. The proposed method is able to depict the successive events that lead to the breakage of biocomposites and it will be a valuable tool to investigate the impact behaviour of other materials as well.

Keywords:
A. Natural Fibers
A. Polymer-matrix composites (PMCs)
B. Impact behaviour
C. Damage mechanics

1. Introduction

Biocomposites with natural fibre reinforcements are considered a potential replacement to traditional structural composites due to their low density, high specific properties, low cost of raw material, relative abundance, and positive environmental profile [1]. Bledzki and Gassan [2], Faruk et al. [3] and Pickering et al. [4] have published extensive review articles on the mechanical behavior of polymer composites reinforced with natural fibres. In particular, it has been reported that composites reinforced with plant fibres from flax plant (*Linum usitatissimum*) in thermoplastic and thermoset matrices have exhibited good specific mechanical properties comparable to those of glass fibre composites [5,6]. However, a lack of data on durability properties of these composites for loading conditions such as fatigue and impact has limited the use of natural fibres for high performance applications [7]. The biocomposite structure may encounter impact loads during their service life due to dropped tools, collisions with loading and unloading fixtures, ballast or cargo and the internal damage produced by such impacts may severely reduce their residual mechanical properties. The difference in impact resistance between biocomposites and traditional composites was investigated by Bos et al. [8] using unnotched Charpy tests and it was reported that the impact strength of short flax fibre compounds were much lower than that of glass fibre. In contrast, Puech et al. [9] showed that PP-hemp biocomposites exhibit higher absorbed energies (up to 40%) than PP-glass composites due to higher strain at break. Recently, several researchers have studied the impact resistance of biocomposites with non-woven short flax fibres in thermoplastic matrix [10] and thermoset matrix [11]. However, the use of natural fibres in structural applications requires higher reinforcement efficiency that can only be achieved with twistless long continuous fibres. The literature on impact resistance of composite laminates with long continuous natural fibres is still limited. There have been some studies on woven hemp fibres [12], jute fibres [13], and unidirectional and cross-ply flax fabric composites [14–16]. Liang et al. [14] found that the fracture mechanism in flax/epoxy composites included delaminations that occurred at low energy level, followed by the development of intra-laminar transverse cracks and macrocracks due to fibre failure. Ravandi et al. [15] investigated the low velocity impact response of continuous flax/epoxy

* Corresponding author.
E-mail addresses: karthik.ramakrishnan@eng.ox.ac.uk (K.R. Ramakrishnan), stephane.corn@mines-ales.fr (S. Corn).
[1] Member of the European Polysaccharide Network of Excellence (EPNOE), http://www.epnoe.eu.

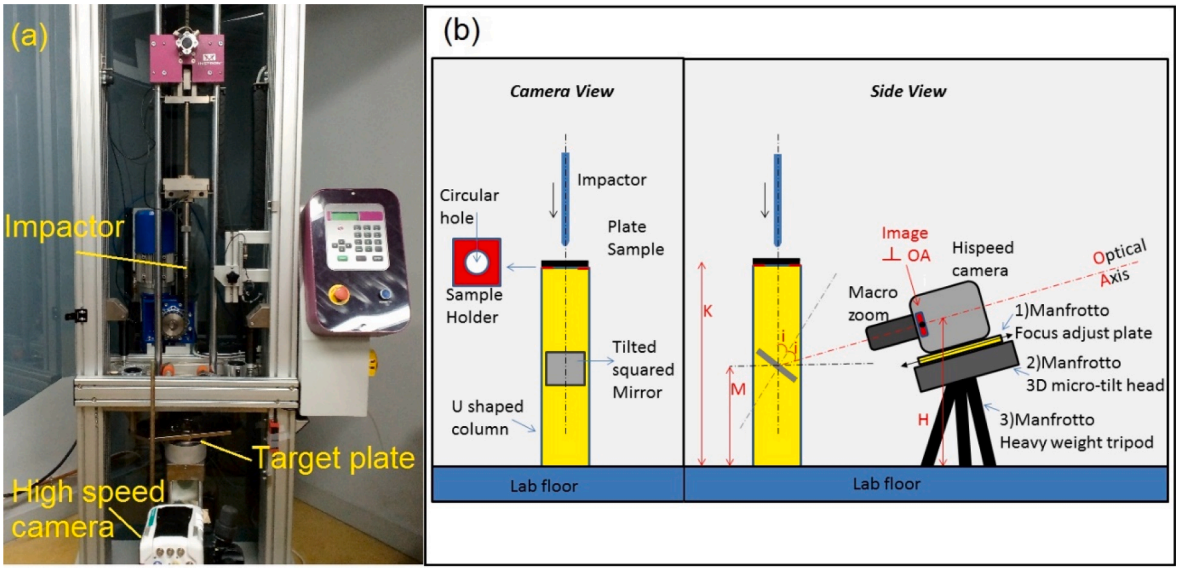

Fig. 1. (a) Drop tower setup used for low velocity impact testing monitored with high speed camera, (b) scheme of the experimental set-up.

composite laminates and found that through-thickness stitching had an adverse effect on the impact resistance as it facilitated the propagation of in-plane cracks. Sy et al. [16] compared the impact performance of unidirectional and cross-ply flax/epoxy laminates and found that the cross-ply laminate had higher penetration threshold energy and impact toughness compared to the unidirectional laminate. One of the limitations of these studies is that there is very limited literature on the comparison of the impact resistance of long continuous natural fibre reinforced composites with thermoset and thermoplastic matrix. In this paper, a comprehensive study on the impact behaviour of woven flax fibre-reinforced composites with epoxy and polypropylene matrix is conducted.

The experimental characterization of impact behaviour of composites is typically conducted using a drop tower. The force–displacement curve obtained from the impact experiment is used to identify the evolution of damage as the creation of damage or cracks results in the sudden loss of stiffness of the specimen and a corresponding drop in the force history. Non-destructive inspection methods such as visual inspection and ultrasonic C-scan are used for the assessment of damage but it is typically conducted after the impact event. For instance, Scarponi et al. [12] used Ultrasonic C-scan to evaluate the damage area in low-velocity impact experiments of plain weave hemp fabric reinforced bio-based epoxy composites. Dhakal et al. [13] used acoustic emission technique to characterize the failure modes of woven jute fibre reinforced unsaturated polyester composite. Santulli [17] developed a method to assess the impact damage in flax-epoxy composites using a combination of hysteresis cycles of the force–deflection curves and optical microscopy. However, the force–displacement data is rarely correlated to the actual creation and propagation of damage. Puech et al. [9] conducted such study using high-speed imaging of the impact response of short hemp fibres reinforced PP. It was found from the video tracking analysis that for a given cumulated crack length, PP-hemp composite absorbed much more energy than PP-glass, which was assumed to be related to differences in failure mechanisms [9]. Flores et al. [18] have shown that high-speed imaging can be used to record strains and deformation as well as crack initiation and propagation during low velocity impact of carbon fibre composites. It is clear that high-speed imaging of the dynamic impact event should provide important information about the impact damage of composites.

Digital Image Correlation (DIC) method is a powerful and flexible optical metrology technique based on digital image processing and numerical computing for the full-field measurements of displacement or strain [19]. Typically, image analysis techniques such as DIC were limited to mostly quasi-static and low strain rate applications for the measurement of surface deformations and has been widely used for the identification of materials constitutive parameters from mechanical tests such as tensile tests. Analysis of stresses in real time during a transient failure event, such as dynamic crack initiation and growth, was challenging due to a combination of spatial and temporal resolution demands such as synchronization difficulties and poor image resolution at high rates [20]. Recent improvements in high speed camera technology have allowed the use of DIC of high-speed images in dynamic event testing [21–24]. Reu and Miller [22] provided an overview of the applications of high-speed DIC used for many experiments including fracture and impact testing. Recently, Pan et al. [23] and Cuynet et al. [24] have also demonstrated the application of high speed imaging for full field measurement in impact testing of composites using a single camera stereo-DIC system and two cameras system, respectively.

The aim of this work is to study the impact behaviour of flax fabrics reinforced biocomposites and to assess the evolution of damages using high-speed imaging coupled with DIC analysis. The high-speed imaging enables the user to better depict the successive events occurring upon the crack propagation. A method to correlate the force-displacement measurements to the cracks propagation during impact test is proposed.

2. Materials and methods

2.1. Manufacturing of composite specimen

Biotex Flax-PP supplied by Composites Evolution, UK was chosen for the thermoplastic composite. Flax/thermoplastic fabric consists of twistless flax fibres and polypropylene (PP) fibres mixed in the ratio of 40/60 (v/v). The commingled fibres are then woven in a balanced 2x2 twill architecture to form fabrics with areal density of 400 g/m^2 [25]. For the thermoset composite, dry flax woven fabrics (Biotex Flax, 400 g/m^2) also supplied by Composites Evolution and a two-part epoxy resin (1800 epoxy resin and 1805 aliphatic amine hardener) supplied by Resoltech Advanced Technology Resins, France were chosen. The resin and the hardener are mixed in the ratio of 100:17 by mass. 10 plies of the flax-PP fabric were used for the thermoplastic composite (flax-PP) while 5 plies of dry flax fabric were used for the thermoset composite (flax-epoxy), so that both biocomposites plates have comparable areal density of flax fibres and thicknesses.

The first step in the manufacturing of the flax-PP biocomposite is the

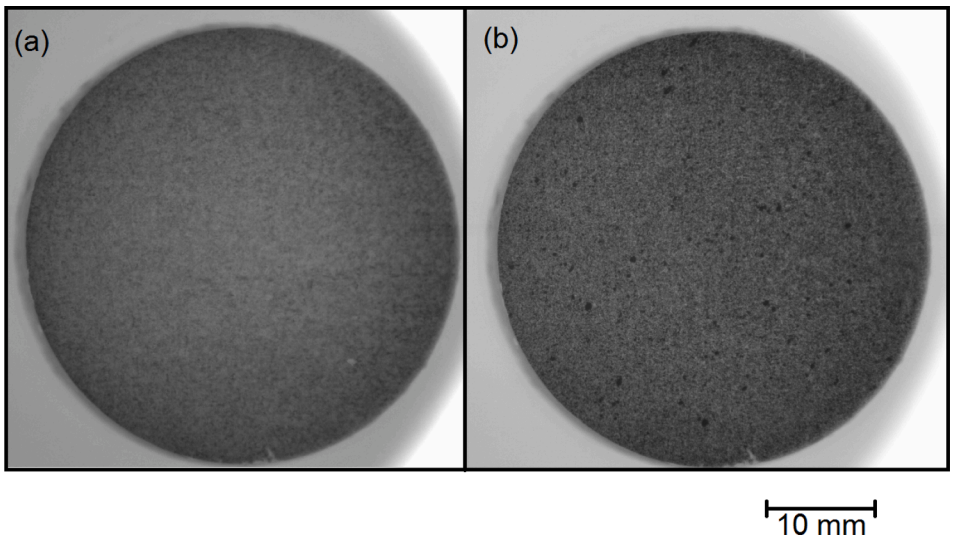

Fig. 2. Typical view of the high-speed camera of the target plate with (a) white powder and (b) fly-speckled pattern.

drying of the fabrics in order to minimize the moisture content. The Biotex Flax-PP fabric was cut to square plies of 300 mm size and dried at 60 °C for 24 h. Ten plies of the fabric were then laid up and then placed between the two rigid steel plates of a hydraulic thermopress. Teflon sheets were used on both steel plates as a mould release surface. The flax-PP composites laminates were processed at a temperature of 210 °C for duration of 10 min. The composite was consolidated at pressure of 40 bars for a final thickness of 3.1 mm ± 0.05 mm. The manufacturing of the flax-epoxy biocomposites followed a similar step of drying, and 140 g of the epoxy resin/hardener mixture was impregnated to the flax fabric in a wet layup process. The five flax fabric plies were stacked and the laminated flax/epoxy composites were hot-pressed under a constant pressure of 20 bars and a constant temperature of 60 °C for 21 h (curing 6 h and post-curing 15 h). The fibre volume fraction of the flax-epoxy composite was estimated from the mass of the dry fabric and resin, and the consolidated plate. The resulting flax-PP and flax-epoxy composites laminates had similar fibre volume fraction (40 %v) and consolidated thickness.

2.2. *Experimental setup for low velocity impact testing*

Low velocity impact testing with velocities below 10 m/s is typically accomplished using a drop tower. Applications for flax composites in the transport industry are expected to involve this velocity regime. The tests were conducted based on standard test method for drop weight impact testing of composites (ASTM D7136) using a CEAST 9350 instrumented drop tower (Instron, UK) shown in Fig. 1. A hemispherical impactor of diameter 20 mm is secured to a carriage assembly weighing 3.1 kg. A composite target plate is clamped in a fixture with 40 mm internal diameter. The carriage is released from an assigned height and falls along guideposts and impacts the target.

A Phantom V2512 high-speed camera (Vision Research, Inc., USA), coupled with long distance macro-zoom lens, was used for slow motion observation of the bottom surface of the composite plates during the impact event. The scheme shown in Fig. 1 b present the camera view and the side view of the experiment. The target plate is placed on a sample holder at the top of a U shaped column and the camera is set up facing and centered on the column. The sample holder has a circular hole to let the impactor go through the sample after rupture and this allows uninterrupted view of the bottom surface of the target plate. A mirror setup placed at an angle below the composite plate allowed the camera to safely capture the impact event and also to shine about 15,000 lm from superLEDs cold light device (VERITAS Constellation 120, USA). The height of the U shaped column is fixed and is defined by K while the height of the center of the camera is given by H, and M is the mirror height placed inside the U shape column. The mirror height M is kept fixed, as it also enables 15000 lx superlum array to shine on the object for short exposure time. The camera is tilted to the correct angle. This angle is reached when the maximum contrast is reached on the whole image (planar sharp focus). Some accurate adjustments of pan, tilt, rotation and slide can be necessary to optimize contrast. As $H > M$, then the mirror angle is adjusted to reach H at the working distance defined by the macrolens zoom (taking into account the reflection path). Optical calibration is performed with optical caliper reference. The scale factor or magnification, which depends on the focal length and the distance between the camera and object, was fixed to 69 µm per pixel. Since the high speed camera coupled with the macro zoom lens has a mass of about 8 kg, a Manfrotto heavy weight tripod 475B (Manfrotto Via Valsugana, 100–36022 Cassola (VI) Italy) was used to ensure stable set-up. This coupling is done by using friction control Pan-Tilt-Rotation Manfrotto tripod head, able to carry the camera weight. The quality of the images has to be perfect to ensure DIC results and so the set-up is improved by adding fine coarse translation Manfrotto 454 micro-positioning sliding plate between the 3D head and the camera. The images were acquired at a frame rate of 39,000 fps and exposure time of 25 µs with a resolution of 786 × 786 pixels. Photoelectronic switches were used to measure the initial velocity (and rebound velocity) of the impactor and also acted as the trigger for the image acquisition in rolling buffer FIFO memory mode.

Image sharpness of the rear surface of the target is determined by maximizing the contrast of the live images while carefully sliding the optical head. In order to create a high contrast zone for the purpose of skeletonisation of the images to monitor the propagation of cracks during the impact of the composite plates, their bottom surface was painted with a thin layer of white powder. Additionally, a black paint was sputtered over the layer of white paint on the bottom surface of one set of the flax composite plates to give it a granular random fly-speckled pattern as shown in the (Fig. 2), which is required for the “pattern matching” based DIC measurements.

The drop height was varied from 0.1 m to 0.3, 0.35, 0.4, and 0.5 m to give a range of kinetic impact energies of 3 J to 15 J. The initial energies were chosen to represent a wide range of damage intensities. The upper bound energy was chosen in order to get experimental results up to the full perforation of the plate. Three specimens were tested at each impact condition to ensure the repeatability of the experiments. The energy absorbed by the composite plate was calculated from the area of the hysteresis loop by integrating the force–displacement curve. The total energy is defined as the energy at peak displacement (i.e. without

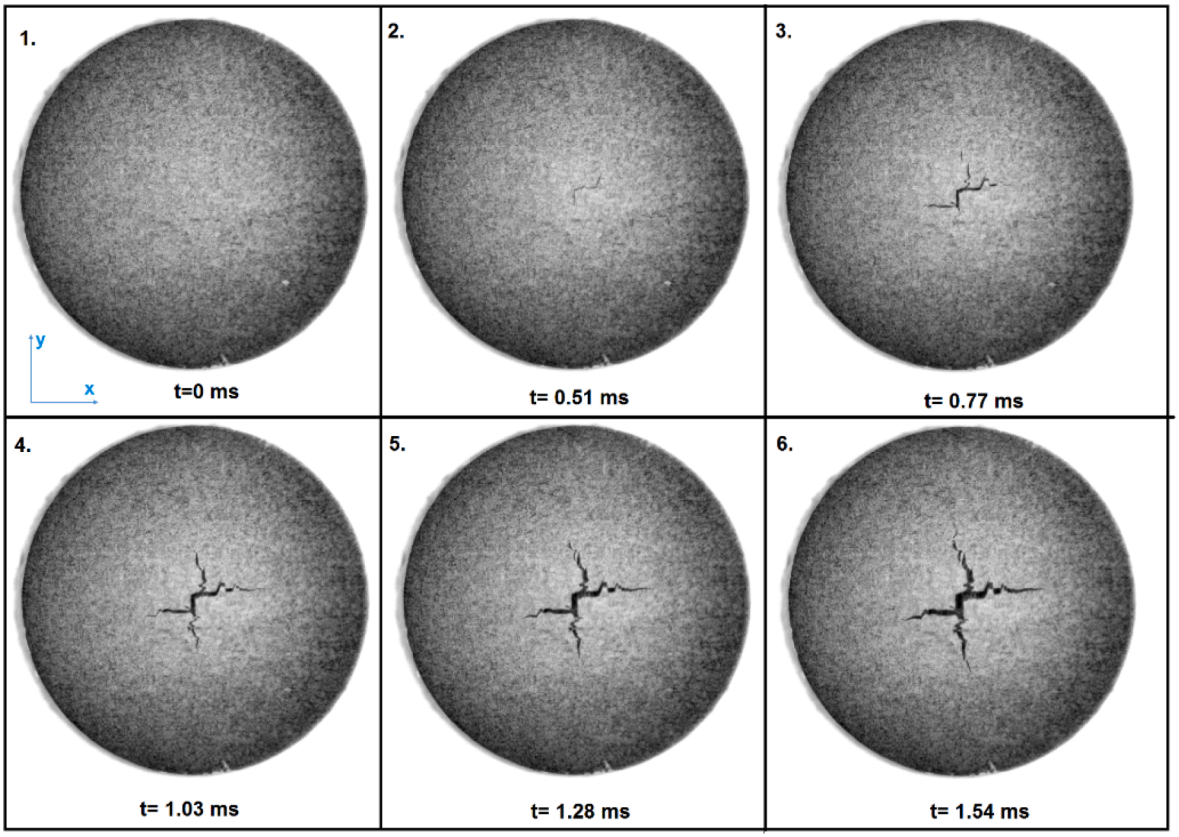

Fig. 3. Typical high-speed video frames showing initiation and propagation of macro-cracks in flax-PP during 6 J impact.

considering the rebound part of the curve). Recovered energy can then be calculated as the difference between the total energy and absorbed energy. It should be noted that not all of the initial kinetic energy of the impactor is available to the plate and some of it is lost in other dissipative losses. Post-impact assessment of the surface deformations and failure mechanisms in the impacted samples were evaluated using an optical 3D measurement system, InfiniteFocus G5 by Alicona (Alicona Imaging Gmbh, Austria). Damage assessment was also conducted by observing cross-sections of the flax-PP and flax-epoxy composite sample using optical microscope. The impacted sample was embedded in coloured resin to preserve the deformed shape and the damage and then the cut section was mounted in a clear epoxy resin. The mounted sample was polished with successively finer abrasive papers and finished with diamond polishing paste.

2.3. *Digital image correlation of high-speed camera images with CinEMA*

Digital image correlation (DIC) analysis was conducted on the images obtained from the high-speed camera. DIC is based on the principle of comparing small zones (or subsets) of the digital images of the specimen surface coated with a random pattern. The image correlation is performed by matching subsets from the reference or undeformed sample and subsequent deformed states to compute full-field displacements and strains. In the 2D DIC of the x-y plane corresponding to the rear surface of the plate, the in-plane displacement fields designated by Ux(x,y) and Uy(x,y) correspond to the displacement that maximizes a similarity criterion between reference and deformed subsets. The image post-processing is based on a three-step DIC approach developed in-house called CinEMA. The definition of the parameters used for the DIC and the details of the algorithm is described in [26,27]. In the first step, the rigid body displacement is calculated by a 2D cross correlation of the selected subimages. In the second step, the DIC processing leads to an incremental displacement evaluation. In-plane displacement fields Ux(x,y) and Uy(x,y) were evaluated at each point of the virtual mesh in the region of interest (ROI) of the sample including the crack zone. The peak of the correlation function was detected at a subpixel accuracy by interpolation and this process is repeated for the entire image to get full-field in-plane displacements. In the third step, the calculation of the displacement gradient around the considered point allows the evaluation of the in-plane Green-Lagrange strain tensor E.

2.4. *Crack-tracking algorithm of high-speed camera images*

High-speed video frames of the bottom surface of a flax-PP plate for a 6 J impact is shown in Fig. 3. The initiation and propagation of macro-cracks at different moments of the impact are observed. It can be seen that at time of 0.77 ms after impact, there is localized damage beneath the point of impact. Radial cracks begin to propagate mainly along the two fibre yarns directions, i.e. 0° and 90°, corresponding to x and y axes.

The DIC analysis is not suitable when discontinuities such as large macroscopic cracks occur, as the measured displacements are no longer associated with the deformation of the material. In order to overcome this limitation, a crack-tracking method is proposed. A macro was written in ImageJ software [28] to detect cracks and measure the cumulative length from each image. The crack-tracking algorithm involves several steps as illustrated in Fig. 4. In the first step, an undamaged reference image is converted to 8-bit and a combination of median and Gaussian blur filters are applied to the image. Next, each image from the high-speed camera was treated with similar filters and subtracted from the reference image to isolate the cracks. The image is converted to mask and binarised and the cracks are clearly visible as black in a white background. A skeletonisation algorithm is then used after different

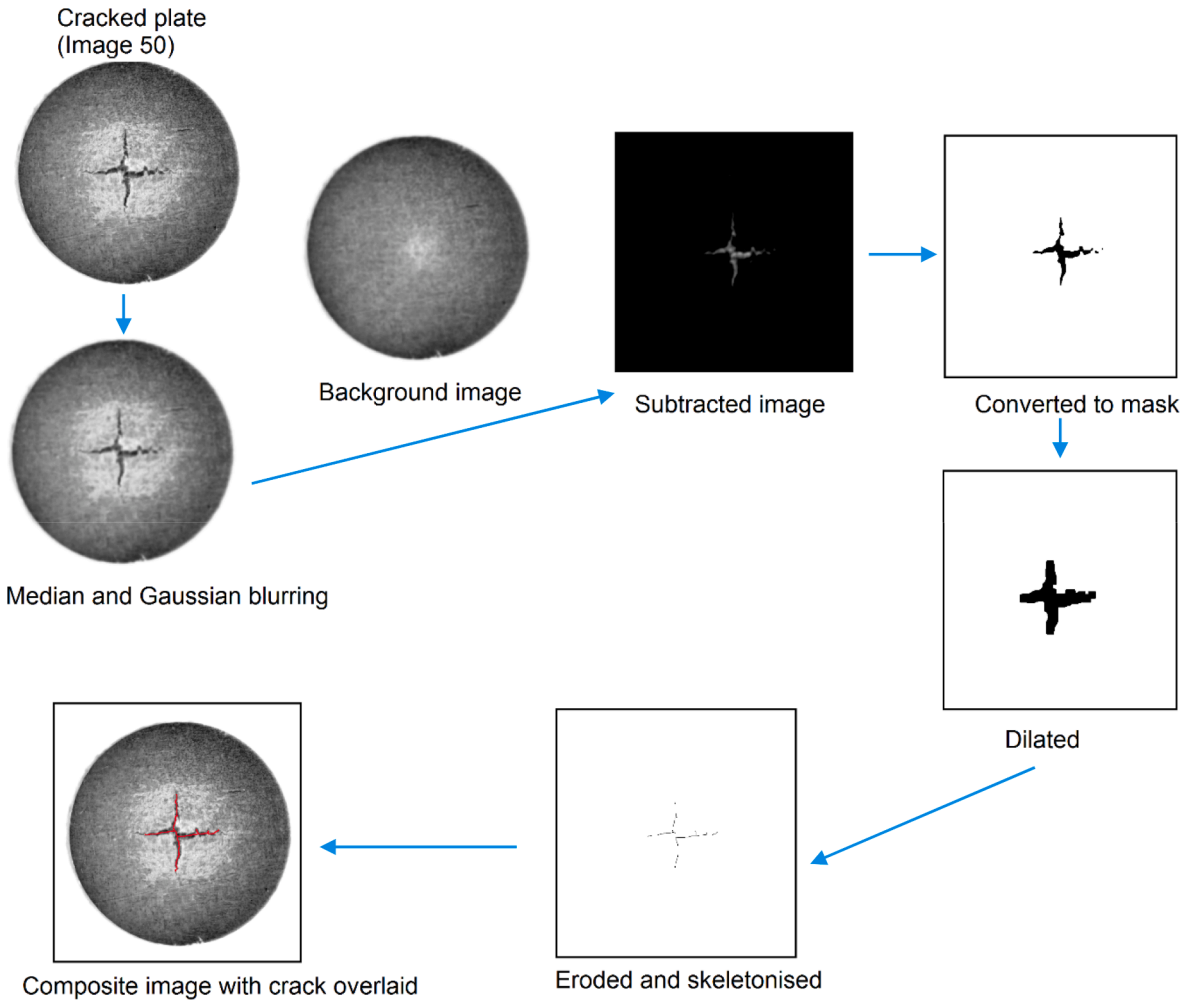

Fig. 4. Procedure for crack-tracking from the high-speed camera images.

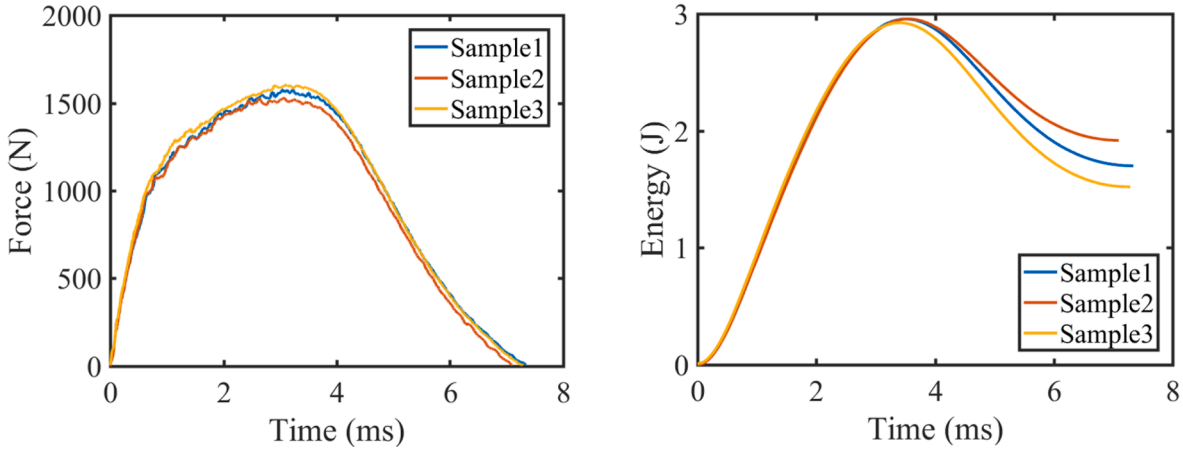

Fig. 5. Typical force-time and energy-time history for 3 J impact of flax-PP composite.

steps of dilation and erosion to highlight the cracks and to trace the crack length with 1-pixel wide lines. The total length of the macro-cracks is measured at each time interval during impact and the evolution of damage observed in the plate was correlated to its force–displacement response. A composite image with the cracks overlaid on the original image is then created to verify that the tracked cracks correspond to the actual damage.

3. Experimental results and discussion

3.1. Drop tower impact testing

The sensor instrumentation in the drop tower allows the measurement of force and displacement history of the impactor during impact. Fig. 5 a shows the typical force history for three flax-PP composite plates

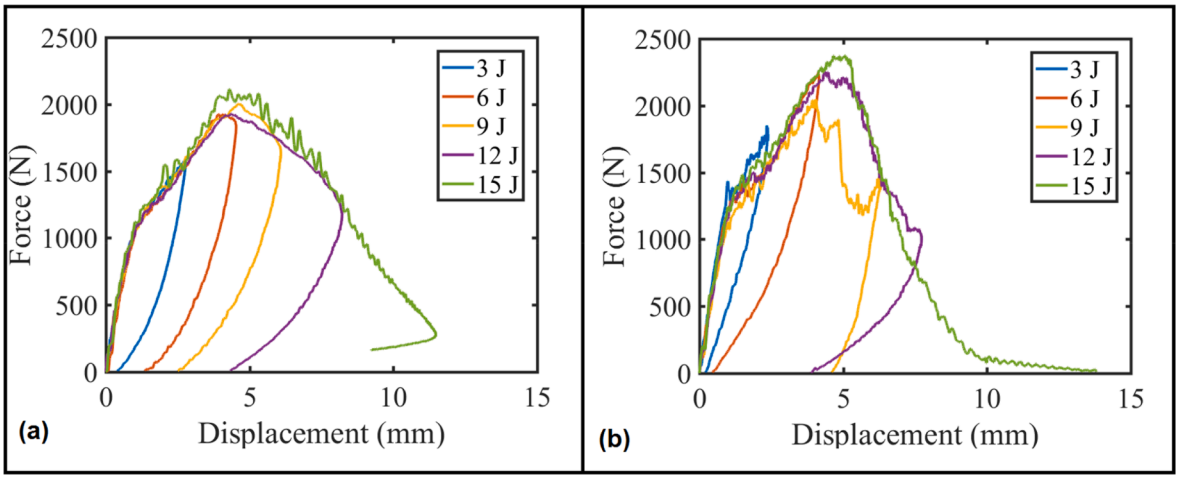

Fig. 6. Comparison of the typical force-displacement curves for different initial impact energies (a) flax-PP composite and (b) flax-Epoxy composite.

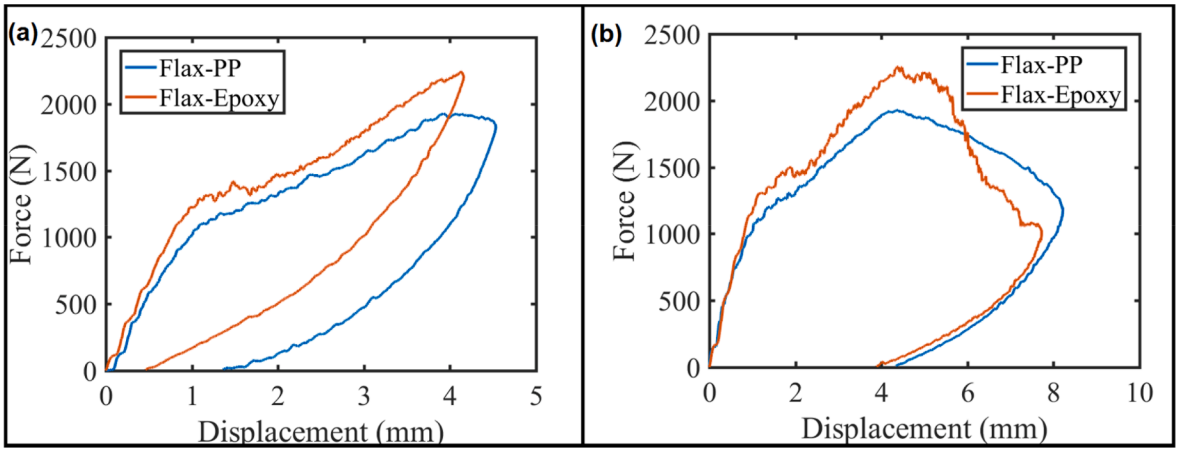

Fig. 7. Comparison of typical Force – displacement curves for (a) 6 J and (b) 12 J impact.

during a 3 J impact. The force curve has an asymmetric bell-shape corresponding to the loading and unloading of the plate. The force response starts with the linear increase up to 1000 N which is followed by a non-linear material behaviour up to peak force of approximately 1550 N. After the peak is reached, there is an unloading phase due to rebound or fracture of the composite. Another significant feature observed from the curves is that the tests are highly repeatable with the three samples showing nearly identical time-histories of force. Fig. 5 b shows the history of the mechanical energy calculated from integrating the force–displacement data. It can be seen that the kinetic energy of the impactor is transferred to the plate during the loading phase of the impact. After the peak is reached, there is a rebound phase where the energy is returned to the impactor. In an ideal elastic impact case, there is a symmetric unloading and all the energy is returned to the impactor. However, it can be seen that there is some energy dissipation and not all the energy transferred to the plate is returned to the impactor. This energy gap results from plastic deformation, viscous dissipation and various damage mechanisms in the composite.

Fig. 6 shows the typical force–displacement curves for impact at different initial impact energies for both the flax-PP and flax-epoxy

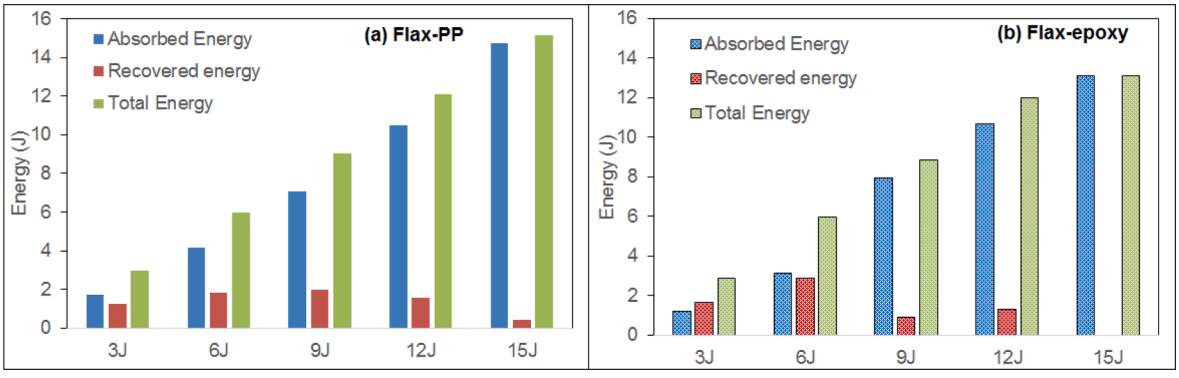

Fig. 8. Comparison of total, absorbed and recovered energies during impact of (a) flax-PP and (b) flax-epoxy composites.

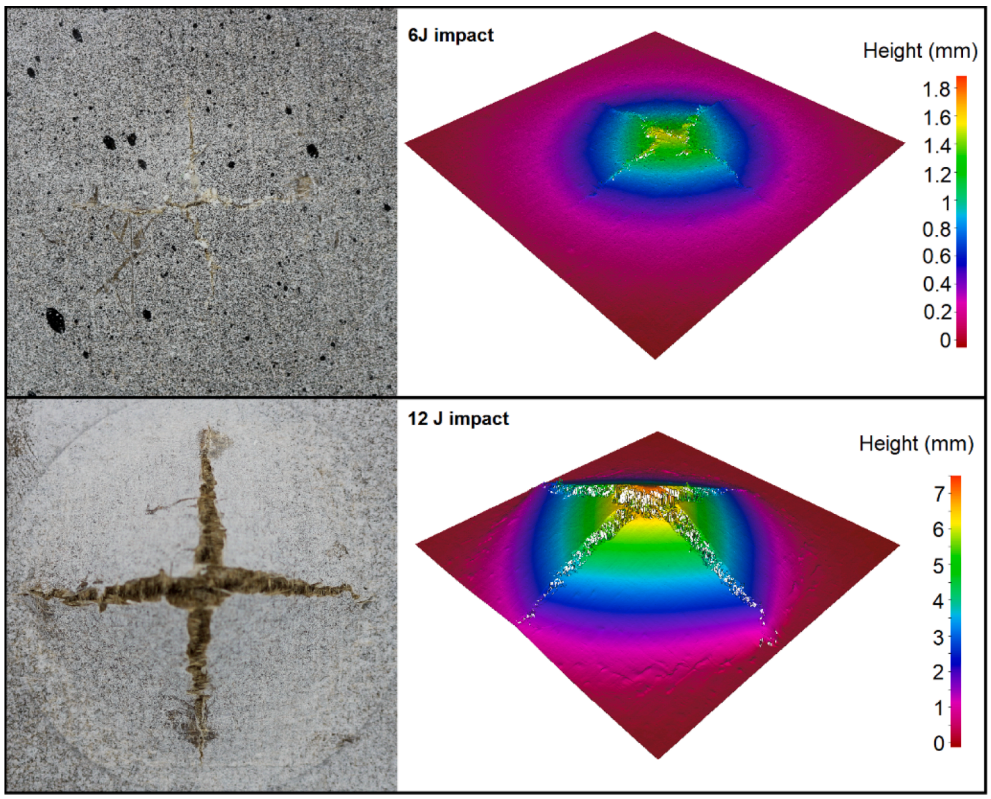

Fig. 9. Visual and profilometer image of post-impact deformation in flax-PP composite after 6 J and 12 J impact.

plates. The impact energy varies from 3 J corresponding to low damage up to full penetration impact at 15 J. A representative sample is shown for each energy as the earlier figure showed that the response is highly repeatable. The initial linear part of the curve is identical for all the loading conditions while the figure shows that the residual displacement after impact increased with impact energy. For impact at 15 J, there is complete perforation of the plate and there is virtually no rebound. The tail in the force response for the perforated sample of flax-epoxy is a

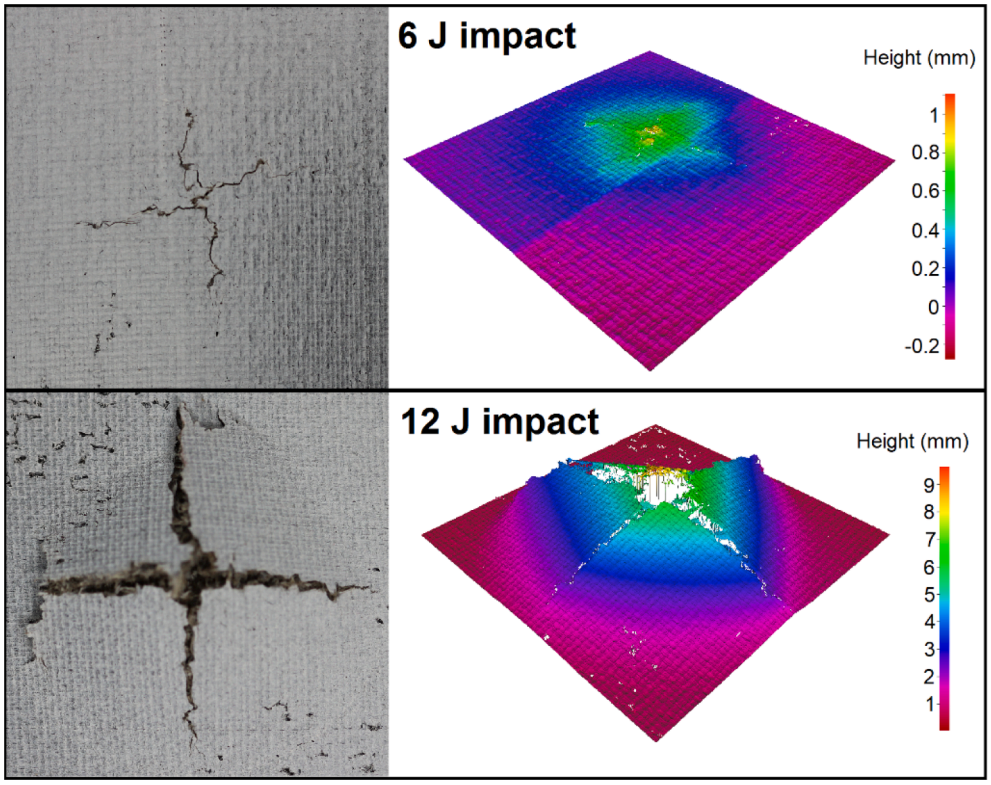

Fig. 10. Visual and profilometer image of post-impact deformation in flax-epoxy composite after 6 J and 12 J impact.

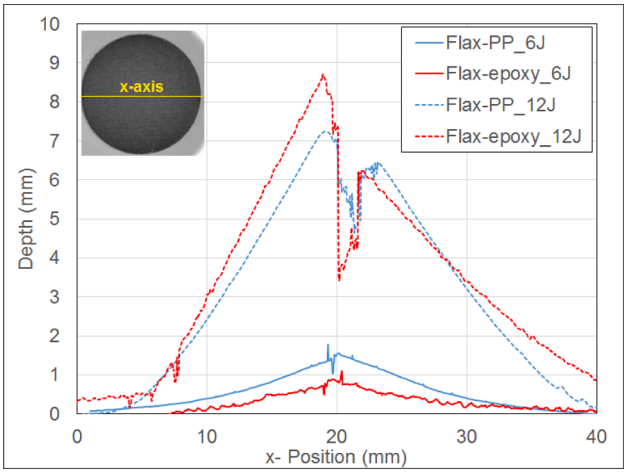

Fig. 11. Depth profile for flax-PP and flax-epoxy composites after 6 J and 12 J impact.

consequence of the residual contact force at the end of impact due to friction between the impactor and the hole in the plate.

A comparison of the typical force–displacement data for a flax-PP and a flax-epoxy composite plates for 6 J and 12 J impact energies is shown in Fig. 7. It can be seen that the two materials exhibited very similar response, suggesting a fibre-dominated behavior of the composites. However, at 6 J, the initial stiffness of the flax-epoxy plate is marginally higher than that of the flax-PP composite due to higher stiffness of the epoxy matrix compared to PP. Besides, it is also evident from the curves that the flax-PP composite has higher maximum displacement for both load cases, which is due to the ductile behaviour of the PP matrix when compared to epoxy.

The absorbed energy calculated from the integration of force–displacement curves are shown in Fig. 8. It can be seen that the absorbed energy increases almost linearly with increasing initial impact energy. However, the recovered energy starts to decrease if perforation failure is initiated, reaching zero for complete penetration of the composite sample. We can estimate the critical energy for penetration failure based on the recovered energy as approximately 9 J for the flax-PP and flax-epoxy composites. A comparison of the energy absorbed by the flax-PP and flax-epoxy composite for different initial impact energies shows that the energy absorbed by the two materials are very similar, with the flax-PP composite absorbing marginally more energy especially for the 3 and 6 J impacts. At higher energies, the two composites show a similar damage response with fibre failure and plate penetration.

3.2. *Visual assessment of impact damage*

A comparison of the visual inspection of the bottom surface of the flax-PP composite samples impacted at energies of 6 J and 12 J is shown in Fig. 9. The profile and topography of the indentations produced by the impact were analyzed by measuring the depth and width of the surface deformations from the Alicona profilometer. Since the polypropylene matrix is a ductile material, extensive deformation is observed in the flax-PP composite as evidenced by the bulged surface and fibre pull-out in the profilometer images. The peak residual deformation of 1.8 and 7.5 mm are observed for the plates impacted at 6 J and 12 J respectively. At lower energies, there is matrix cracking around the point of impact and as the energy of impact increases, fibre fracture forms a crack that is aligned with the fibre directions of 0 and 90°. There is extensive fibre failure of the composite for initial energy of 12 J for the flax-PP composite and it can be seen that the crack nearly reaches the edge of the

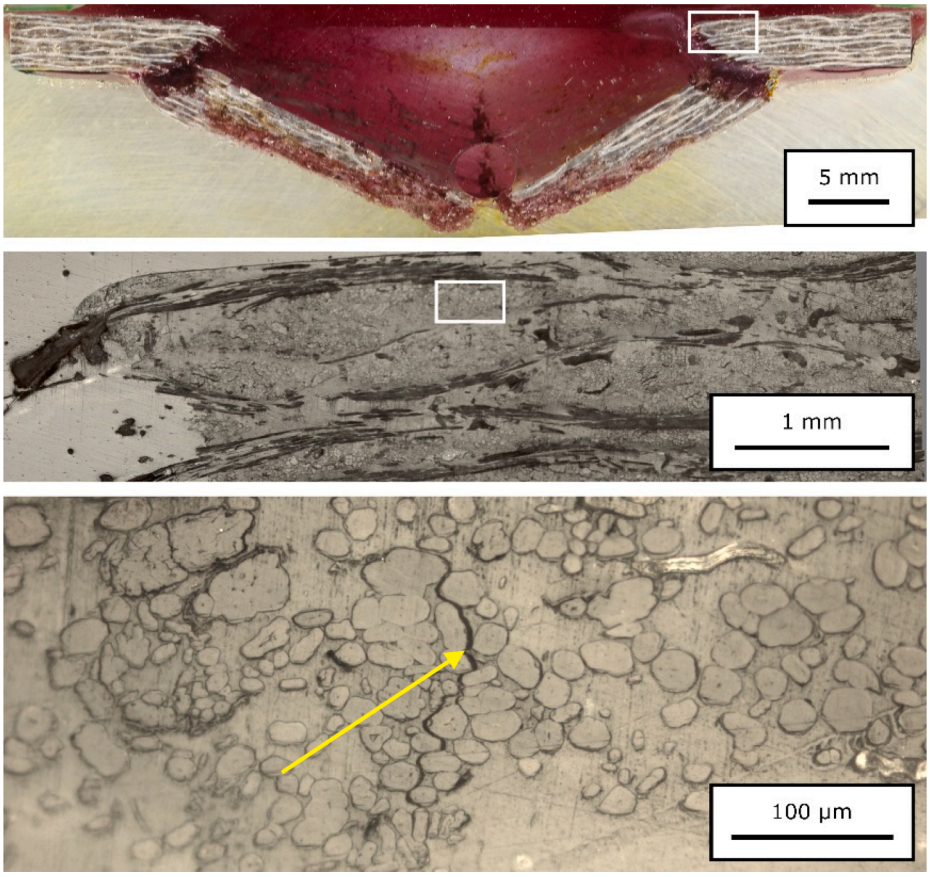

Fig. 12. Optical microscope images of the cross-section of flax-PP composite plate in the damage zone after 12 J impact.

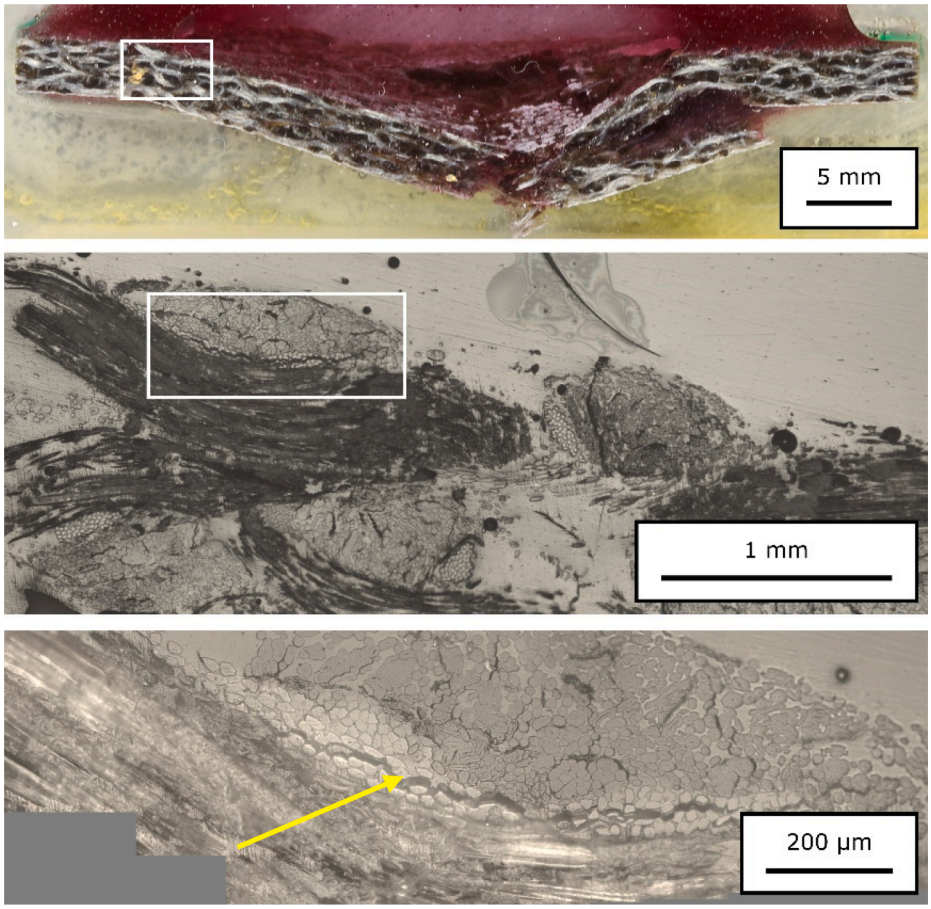

Fig. 13. Optical microscope images of the cross-section of flax-epoxy composite plate in the damage zone after 12 J impact.

clamping fixture.

Similar analysis of the flax-epoxy composite is shown in Fig. 10 and the profilometer data for the 6 J impact shows that due to the brittle behaviour of the epoxy matrix, the permanent deformation is not as pronounced as in the thermoplastic composite. For the 6 J impact, the peak residual displacement is only 1.1 mm. The fibre fracture at the centre of the impact zone is similar to the flax-PP composite. It can been seen that there is complete penetration of the flax-epoxy composite for the 12 J impact.

The depth profiles of the rear of the impacted plate obtained from the profilometer is compared for the 6 J and 12 J impacts of flax-PP and flax-epoxy composites in Fig. 11. Since the deformation of the plate is symmetric, the depth is plot along the central line of only one axis. It can be seen that the depth is highest at the center of the impacted area (20 mm), with 0 and 40 mm representing the clamped edge. The overall depth profile is similar for the flax composites with PP and epoxy matrix but it can be seen that the epoxy composite has less permanent deformation than the ductile PP matrix for the 6 J impact while at the higher energy there is complete perforation in both plates seen as discontinuities in the depth profile.

Optical microscope images at different magnifications of the cross-section of the flax-PP composite impacted at 12 J are shown in Fig. 12. It can be seen that there is a large impact crater and fibre fracture within the composite. Higher magnification images show the presence of matrix damage in addition to the fibre failure with evident matrix cracks through the flax fibre bundles. It is known that the limited wettability of natural fibres towards apolar and viscous matrices such as PP leads to poor impregnation and the formation of micro and macro-pores. Ramakrishnan et al. [25] calculated the porosity volume fraction from X-ray computed tomography analysis and reported that the pressure and temperature of the manufacturing process have a strong influence on the formation of pores. It has also been reported [29] that surface treatments can be successfully used to increase the interactions between natural fibres and polymer matrices, and significantly enhance the interfacial adhesion leading to better stiffness and possibly modifying impact strength properties.

In the case of the cross-section of the flax-epoxy composites in Fig. 13, it can be seen in the higher magnification image that transverse matrix cracks (highlighted by arrow) lead to delamination type failure between the plies of the composite, which was not visible in the case of flax-PP composite. This is consistent with the complex fracture mechanisms observed in the micrographs of impacted flax epoxy plates [14], where a combination of delamination and transverse cracking were reported near the specimen rear face. This highlights a more cohesive behavior for flax-epoxy composite with crack propagation perpendicular to the impact direction, i.e. delamination. It was also reported that the damage in the rear face of flax/epoxy laminates is principally fibre breakage with limited delamination suggesting a fibre-dominant rather than matrix-controlled damage [16].

3.3. *Results of digital image correlation analysis*

The displacement contours and strain distributions obtained from the Digital Image Correlation for the flax - PP composites impacted at 6 J are shown in Fig. 14. The image is at time of 0.54 ms from the beginning of the impact (21st image), which corresponds to the initiation of the cracking as clearly identified by the DIC program. It can be seen that the Ux and Uy displacement fields are qualitatively similar showing that the 2D-DIC is able to compute the full-field displacement of the plate. The strain contours show the initiation of cracks as strain localization and it

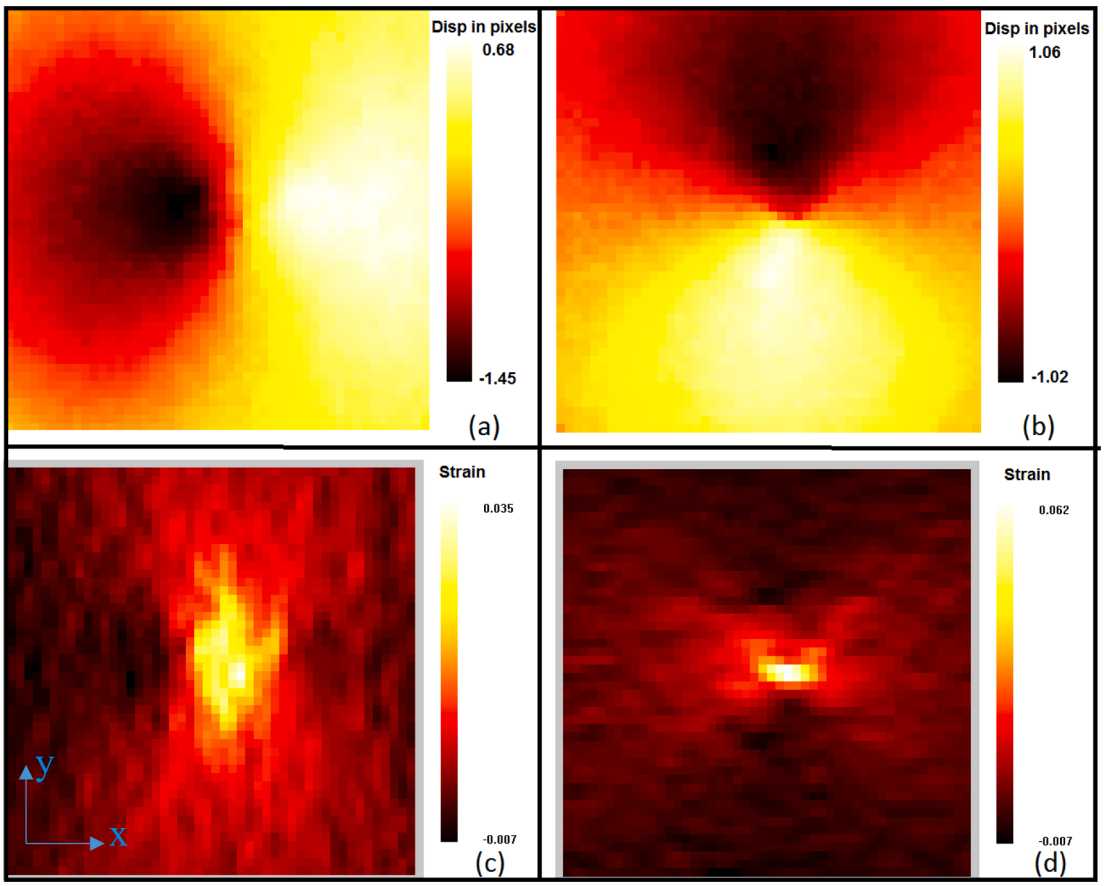

Fig. 14. (a) and (b) : Contours of Ux and Uy displacements; (c) and (d) : contours of xx and yy strains components; for flax-PP composite. (time = 0.54 ms; 21st image).

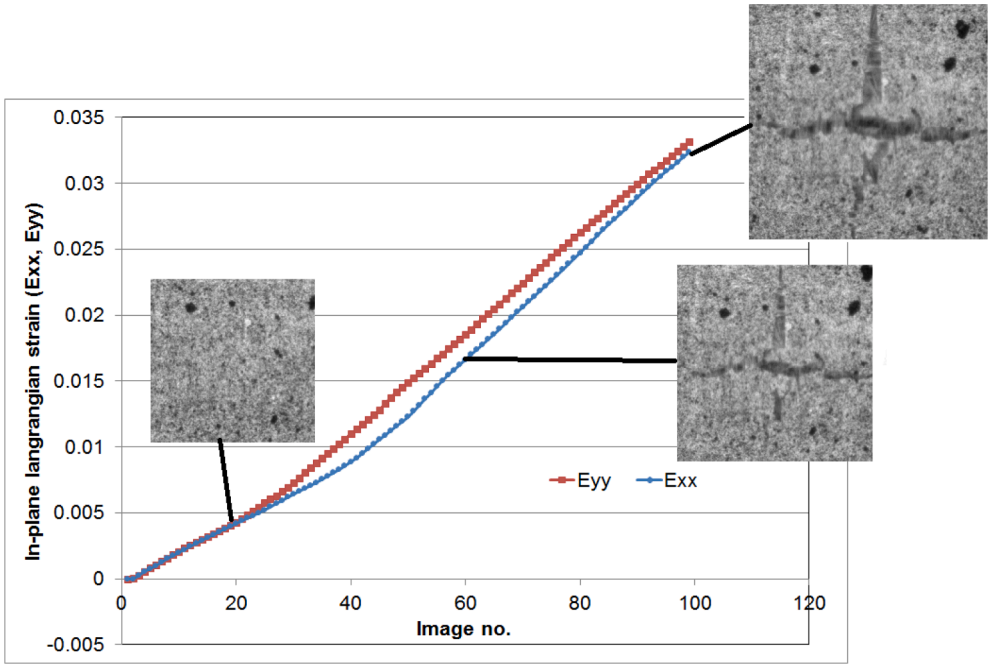

Fig. 15. Lagrangian strains calculated by DIC method for 6 J impact on flax-PP composite, with cropped views of the plate bottom surface.

can be seen that at the point of initiation, the cracks are not symmetric in the × and y directions.

Fig. 15 shows the strain history from the center of flax-PP composite for 6 J impact case. It can be seen that the strain values in the xx-direction and yy-direction closely follow one another, supporting the biaxial loading response of the composite plate. The response diverges

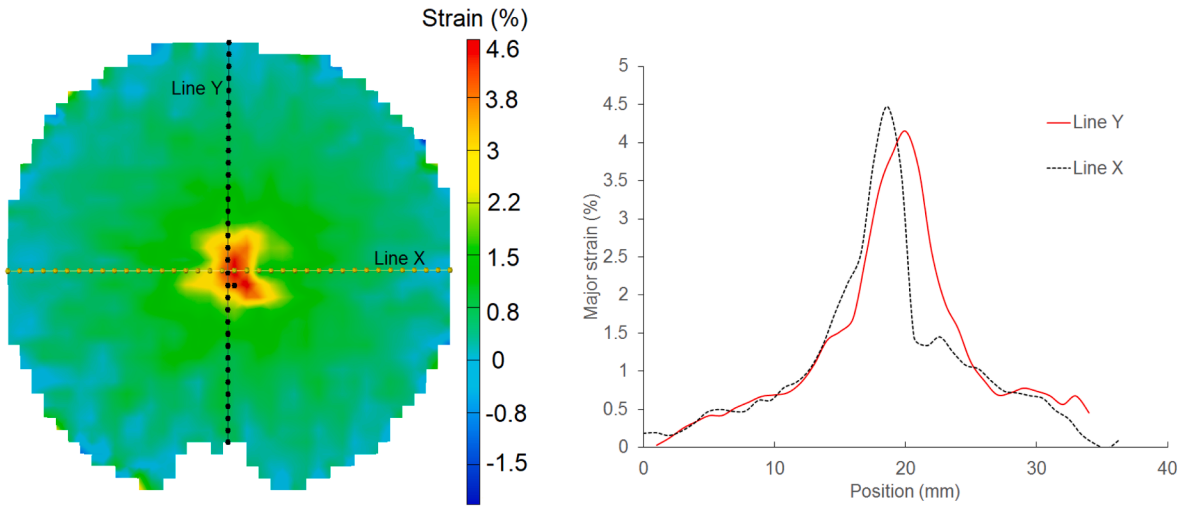

Fig. 16. Strain contours in the xx and yy directions for flax-epoxy composite (6 J impact).

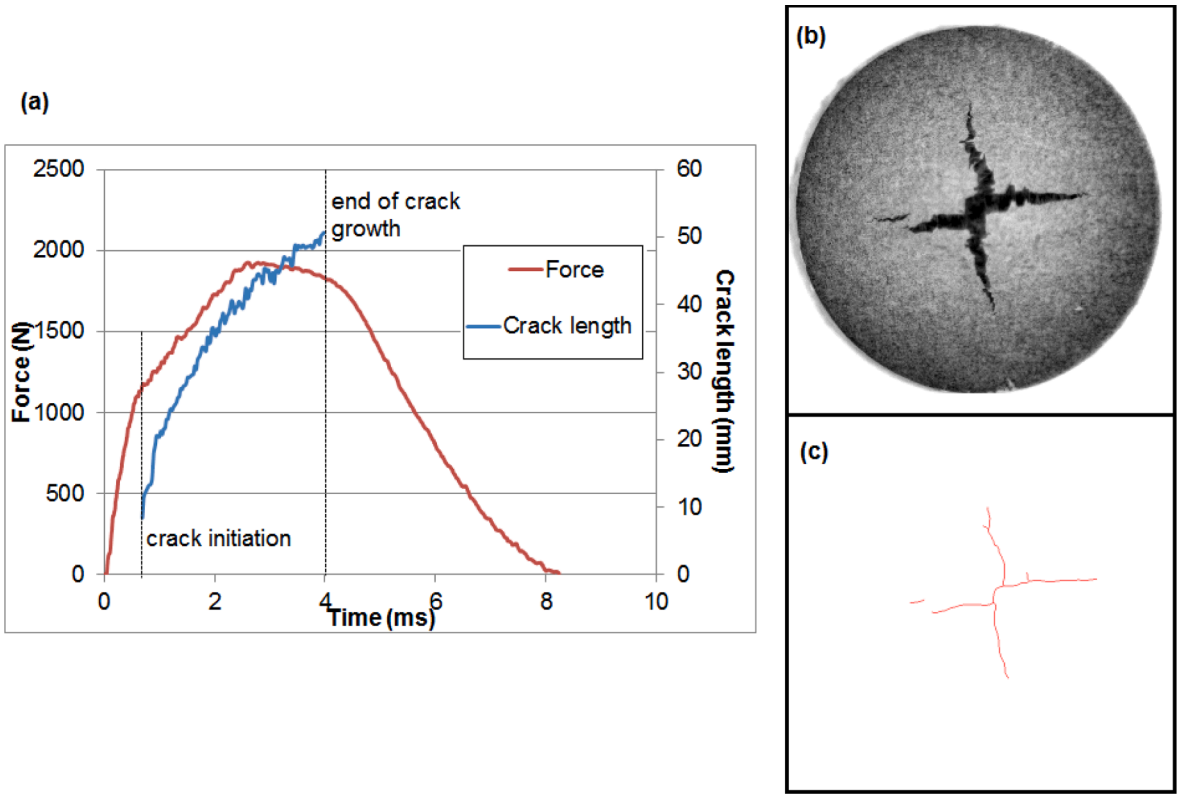

Fig. 17. (a) Force – displacement curves for 6 J impact on Flax-PP composite, along with total crack length; (b) Real time high-speed image of the plate at maximum crack length; (c) Skeletonised image of the crack.

from each other at the initiation of the cracks, as the cracks are not formed in the x and y – directions at the same moment. This is supported in the strain contours of Fig. 14. However, the response stabilizes after the crack propagates to a certain length.

A similar DIC analysis was conducted on flax-epoxy composite for impact of 6 J and results are shown in Fig. 16. The major strain contour is for image 14 after the first contact and just before the beginning of cracks. It can be seen that the strain response of the plate is symmetric at this time with a sharp peak at the centre of the plate and gradually decreasing to the edges. It should be noted again that the subset matching algorithm of the DIC method is not capable of calculating strain histories when there are discontinuities due to the cracks and fibre failures. Therefore the DIC method is applicable only for lower energy impacts before the displacement discontinuities induced by the creation of macro-cracks on the surface.

The advantage of the DIC analysis is that it is possible to obtain full-field displacement measurement of the impacted plate which is useful when there is strain localization. In heterogeneous materials such as composites, it is important to have the local deformation history in addition to the global response. This is a promising methodology for studying the damage evolution in biocomposites. However, there are still some significant challenges regarding the use of high-speed camera and DIC for impact damage assessment. One of the main problems is that the out-of-plane displacement of the specimen during impact leads to a

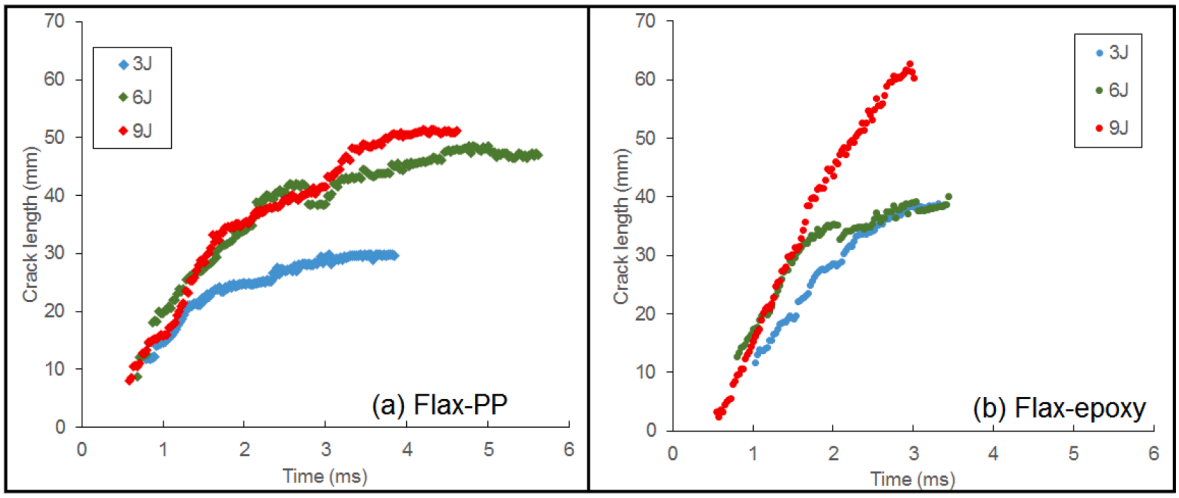

Fig. 18. Comparison of crack lengths for 3, 6 and 9 J impact of (a) flax-PP and (b) flax-epoxy composite.

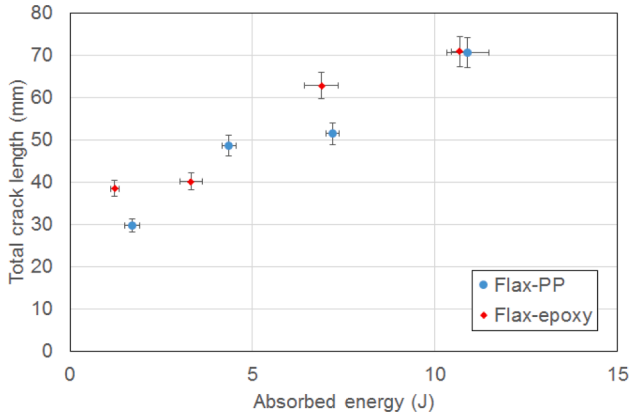

Fig. 19. Comparison of total crack lengths vs. absorbed energy for flax-PP and flax-epoxy composites.

change in the image-to-object distance [30]. It is possible that the magnification of the images will change considerably due to the out-of-plane displacement, which will lead to errors in the calculation of in-plane displacements. Even though out-of-plane displacement during the impact can cause a strain error in the 2D DIC measurements. A stereo DIC based on the principle of binocular stereovision can help overcome this problem. Pankow et al. [31] have shown that large out-of-plane displacements can be captured by a 3D DIC system. It would be interesting to adapt this stereo-correlation system for impact assessment in the future. Nevertheless, Reu and Miller [22] pointed out that despite its drawbacks, two-dimensional information is more than adequate in a number of applications.

3.4. Crack-tracking during impact

Fig. 17 shows the evolution of cumulative crack length correlated to the force–time history obtained from the sensors. The force response exhibits an initial linear region followed by softening phase where the stiffness changes and it can be observed that the initiation of crack corresponds to the stiffness change at critical force of 1100 N. The crack length continues to increase as the crack propagates along the principal directions and reaches a maximum at the end of the loading phase. It should be noted that this is the total crack length and not the length of each radial arm. The kinematics of the crack propagation can be observed with this crack tracking method which is a significant difference to published literature such as Sy et al. [16] who only report the post-impact total crack length.

A comparison of the crack evolution curves for flax-PP and flax-epoxy composites impacted at different energies is shown in Fig. 18. It can be seen that the crack length is initiated approximately 0.6 ms after the start of impact and increases to a maximum length which depends on the impact energy and also the materials. Indeed, there are some significant differences between the evolution of crack lengths for the flax composite with thermoplastic and thermoset matrix. The flax-PP composite reaches a maximum crack length of 29 mm, 47 mm and 51 mm for 3, 6 and 9 J impacts, respectively. On the other hand, the flax-epoxy composite reaches maximum crack length of 38, 40 and 61 mm for the same initial impact energies. It is noticeable that cracks propagation is much faster in the brittle epoxy matrix compared to the more ductile PP matrix, maximum crack length being thus reached at shorter time.

The total crack length for the different energy impacts is plotted against the absorbed energy in Fig. 19. This shows that for a given crack length, the flax-PP and flax-epoxy composites absorb similar amount of energy, indicating that despite the differences in failure mechanisms for the two composites, there is no significant effect on the quantity of energy absorbed per length of cracks by changing the matrix from epoxy to PP (with very different mechanical properties). This proves the potential of commingled thermoplastic biocomposite with shorter manufacturing cycle and lower density to have similar impact performance as the flax-epoxy composite. The ductility of the PP matrix has the potential to further improve the impact performance if the fibre–matrix interface can be improved by optimized manufacturing conditions and fibre treatments.

4. Conclusions

The aim of the paper was to compare the impact behaviour of biocomposites reinforced with flax fibres in thermoplastic and thermoset matrices. A compression moulding process was used to manufacture flax-PP and flax-epoxy composite plates with similar fibre volume fraction and areal density. A drop tower system was used to conduct impact tests at multiple energies, and force and displacement histories were measured during impact. Additionally, a high-speed image acquisition system was used to observe the rear surface of the target to evaluate the damage kinematics in the composite. The different modes of damage and the critical energy required for complete penetration were identified for the composite. The key findings of the paper are:

1. Comparison of the impact response shows that the performance of the flax fibre reinforced composite was similar for the thermoset and thermoplastic matrix. The flax-PP composite exhibits more ductile

behavior and absorbs slightly more energy than the thermoset composite, while a more cohesive behavior was observed for flax-epoxy composite with the appearance of delamination type failure.
2. The optical instrumentation implemented in this study shows that the initiation of damage cannot be clearly identified simply from the force–displacement curve (as it is usually performed). Therefore, the assessment of damage requires the support of a local analysis, which was implemented in this work.
3. A method was proposed to use high-speed imaging for in-situ observation of the creation and propagation of damages in natural fibre-reinforced composites. A macro was implemented in ImageJ software so as to measure cracks lengths from images obtained from Phantom high-speed camera. The cumulative crack length was evaluated at each time interval and the evolution of damage observed in the plate during impact was correlated to the force–displacement response. The maximum crack length for flax-PP composite was 29 mm, 47 mm and 51 mm for 3, 6 and 9 J impacts, respectively, while the flax-epoxy composite reached maximum crack length of 38, 40 and 61 mm for the same initial impact energies.
4. In literature, the DIC technique has been used previously to measure the mechanical properties in quasi-static strain rates but their use for high-speed image processing has been limited. In our study, we applied DIC technique during impact on samples coated with white paint and with speckled patterns. The displacement contours and strain distributions were calculated using in-house program CinEMA. From the strain contours, it was possible to identify strain localization and the initiation of the cracking.
5. One of the main outcomes of this work is that, in addition to the post-mortem damage assessment of the impacted composites, it is possible to follow the damage kinematics over time with the high-speed camera.

The proposed method better depicts the successive events that lead to the breakage of composites and can be a valuable tool to study the impact behaviour of not only natural fibre-reinforced composites but other materials as well. Future study will utilize high-speed imaging with stereo-correlation to take into account out-of-plane displacement. The development of a Finite Element model of the impact behaviour of flax biocomposites and a comparison of the simulated and experimental results is also under study.

CRediT authorship contribution statement

Karthik Ram Ramakrishnan: Conceptualization, Methodology, Investigation. **Stéphane Corn:** Conceptualization, Methodology, Investigation, Supervision. **Nicolas Le Moigne:** Conceptualization, Methodology, Investigation, Supervision. **Patrick Ienny:** Conceptualization, Methodology, Investigation. **Pierre Slangen:** Conceptualization, Methodology, Investigation.

Declaration of Competing Interest

The authors declare that they have no known competing financial interests or personal relationships that could have appeared to influence the work reported in this paper.

Acknowledgements

This project was funded by the European Union's Horizon 2020 Programme (HERMES project, grant agreement n° 636520). KRR also acknowledges Mr. Jere Ahkiola for his assistance with profilometer and optical microscope imaging.

References

[1] Shah DU, Schubel PJ, Clifford MJ. Can flax replace E-glass in structural composites? A small wind turbine blade case study. Compos. Part B Eng. 2013;52:172–81. https://doi.org/10.1016/j.compositesb.2013.04.027.
[2] Bledzki JGAK. Composites reinforced with cellulose based fibre. Prog. Polym. Sci. 1999;24:221–74.
[3] Faruk O, Bledzki AK, Fink H-P, Sain M. Biocomposites reinforced with natural fibers: 2000–2010. Prog. Polym. Sci. 2012;37(11):1552–96. https://doi.org/10.1016/j.progpolymsci.2012.04.003.
[4] Pickering KL, Efendy MGA, Le TM. A review of recent developments in natural fibre composites and their mechanical performance. Compos. Part A Appl. Sci. Manuf. 2016;83:98–112.
[5] Yan L, Chouw N, Jayaraman K. Flax fibre and its composites – A review. Compos. Part B Eng. 2014;56:296–317. https://doi.org/10.1016/j.compositesb.2013.08.014.
[6] Pil L, Bensadoun F, Pariset J, Verpoest I. Why are designers fascinated by flax and hemp fibre composites? Compos. Part A Appl. Sci. Manuf. 2016;83:193–205. https://doi.org/10.1016/j.compositesa.2015.11.004.
[7] Bensadoun F, Depuydt D, Baets J, Verpoest I, van Vuure AW. Low velocity impact properties of flax composites. Compos. Struct. 2017;176:933–44. https://doi.org/10.1016/j.compstruct.2017.05.005.
[8] Bos HL, Müssig J, van den Oever MJA. Mechanical properties of short-flax-fibre reinforced compounds. Compos. Part A Appl. Sci. Manuf. 2006;37(10):1591–604. https://doi.org/10.1016/j.compositesa.2005.10.011.
[9] Puech L, Ramakrishnan KR, Le Moigne N, Corn S, Slangen PR, Duc AL, Boudhani H, Bergeret A. Investigating the impact behaviour of short hemp fibres reinforced polypropylene biocomposites through high speed imaging and finite element modelling. Compos. Part A Appl. Sci. Manuf. 2018;109:428–39. https://doi.org/10.1016/j.compositesa.2018.03.013.
[10] Truong Hoang T-Q, Touchard F. Non-woven flax fiber reinforced polypropylene : mechanical properties in static and low velocity impact behaviours. Polym. Polym. Compos. 2013;21(5):259–70.
[11] Habibi M, Laperrière L, Hassanabadi HM. Influence of low-velocity impact on residual tensile properties of nonwoven flax/epoxy composite. Compos Struct 2017;186(May):175–82. https://doi.org/10.1016/j.compstruct.2017.12.024.
[12] Scarponi C, Sarasini F, Tirillò J, Lampani L, Valente T, Gaudenzi P. Low-velocity impact behaviour of hemp fibre reinforced bio-based epoxy laminates. Compos. Part B Eng. 2016;91:162–8. https://doi.org/10.1016/j.compositesb.2016.01.048.
[13] Dhakal HN, Arumugam V, Aswinraj A, Santulli C, Zhang ZY, Lopez-Arraiza A. Influence of temperature and impact velocity on the impact response of jute/UP composites. Polym Test 2014;35:10–9. https://doi.org/10.1016/j.polymertesting.2014.02.002.
[14] Liang S, Guillaumat L, Gning P-B. Impact behaviour of flax/epoxy composite plates. Int. J. Impact Eng. 2015;80:56–64. https://doi.org/10.1016/j.ijimpeng.2015.01.006.
[15] Ravandi M, Teo WS, Tran LQN, Yong MS, Tay TE. Low velocity impact performance of stitched flax/epoxy composite laminates. Compos. Part B Eng. 2017;117:89–100. https://doi.org/10.1016/j.compositesb.2017.02.003.
[16] Sy BL, Fawaz Z, Bougherara H. Damage evolution in unidirectional and cross-ply flax/epoxy laminates subjected to low velocity impact loading. Compos. Part A Appl. Sci. Manuf. 2018;112(March):452–67. https://doi.org/10.1016/j.compositesa.2018.06.032.
[17] Santulli C. Falling weight impact damage characterisation on flax / epoxy laminates. Int. J. Mater. Prod. Technol. 2009;36(1999):221–8.
[18] Flores M, Mollenhauer D, Runatunga V, Beberniss T, Rapking D, Pankow M. High-speed 3D digital image correlation of low-velocity impacts on composite plates. Compos B Eng 2017;131:153–64. https://doi.org/10.1016/j.compositesb.2017.07.078.
[19] Pan B. Digital image correlation for surface deformation measurement: historical developments, recent advances and future goals. Meas. Sci. Technol. 2018;29(8). https://doi.org/10.1088/1361-6501/aac55b.
[20] Kirugulige MS, Tippur HV, Denney TS. Measurement of transient deformations using digital image correlation method and high-speed photography: application to dynamic fracture. Appl. Opt. 2007;46(22):5083. https://doi.org/10.1364/AO.46.005083.
[21] Tiwari V, Williams S. Application of digital image correlation in impact testing. SEM Annu Conf Expo Exp Appl Mech, vol. 1, no. Ccd, pp. 2–3, 2005, [Online]. Available: http://sem-proceedings.com/05s/sem.org-2005-SEM-Ann-Conf-s025p2-Application-Digital-Image-Correlation-Impact-Testing.pdf.
[22] Reu PL, Miller TJ. The application of high-speed digital image correlation. J. Strain Anal. Eng. Des. 2008;43(8):673–88. https://doi.org/10.1243/03093247JSA414.
[23] Pan B, Yu L, Yang Y, Song W, Guo L. Full-field transient 3D deformation measurement of 3D braided composite panels during ballistic impact using single-camera high-speed stereo-digital image correlation. Compos. Struct. 2016;157:25–32. https://doi.org/10.1016/j.compstruct.2016.08.017.
[24] Cuynet A, Scida D, Roux É, Toussaint F, Ayad R, Lagache M. Damage characterisation of flax fibre fabric reinforced epoxy composites during low velocity impacts using high-speed imaging and Stereo Image Correlation. Compos. Struct. 2018;202(May):1186–94. https://doi.org/10.1016/j.compstruct.2018.05.090.
[25] Ramakrishnan KR, Le Moigne N, De Almeida O, Regazzi A, Corn S. Optimized manufacturing of thermoplastic biocomposites by fast induction-heated compression moulding: Influence of processing parameters on microstructure development and mechanical behaviour. Compos A Appl Sci Manuf 2019;124:105493. https://doi.org/10.1016/j.compositesa:2019.105493.

[26] Ivanov E, Ienny P, Leger R, Caro-Bretelle AS, Kotsilkova R. Strain Localisation in iPP/MWCNT Nanocomposites Using Digital Image Correlation: Strain Localisation in iPP/MWCNT Nanocomposites. Strain 2014;50(1):37–47. https://doi.org/10.1111/str.12065.
[27] Christmann A, Ienny P, Quantin JC, Caro-Bretelle AS, Lopez-Cuesta JM. Mechanical behaviour at large strain of polycarbonate nanocomposites during uniaxial tensile test. Polymer (Guildf) 2011;52(18):4033–44. https://doi.org/10.1016/j.polymer.2011.06.056.
[28] Ferreira T, Rasband W. ImageJ User Guide. http://doi.org/10.1038/nmeth.2019.
[29] Le Moigne N, Otazaghine B, Corn S, Angellier-coussy H, Bergeret A. Surfaces and Interfaces in Natural Fibre Reinforced Composites Fundamentals , Modifications and Characterization. Springer briefs in molecular science, 2018.
[30] Pan B, Qian K, Xie H, Asundi A. Two-dimensional digital image correlation for in-plane displacement and strain measurement: A review. Meas. Sci. Technol. 2009; 20(6). https://doi.org/10.1088/0957-0233/20/6/062001.
[31] Pankow M, Justusson B, Waas AM. Three-dimensional digital image correlation technique using single high-speed camera for measuring large out-of-plane displacements at high framing rates. Appl. Opt. 2010;49(17). https://doi.org/10.1364/AO.49.003418.